Effect of Ethylene Glycol, Urea, and N-Methylated Glycines on DNA Thermal Stability: The Role of DNA Base Pair Composition and Hydration†

Larisa J. Nordstrom,‡ Chris A. Clark,‡ Brian Andersen,§ Sara M. Champlin,|| and Jeffrey J. Schwinefus*,‡

Department of Chemistry, St. Olaf College, Northfield, Minnesota 55057, Laboratory of Membrane Biochemistry and Biophysics, National Institute on Alcohol Abuse and Alcoholism, National Institutes of Health, 5625 Fishers Lane, Rockville, Maryland 20892, and School of Medicine, Washington University in St. Louis, St. Louis, Missouri 63110

Received December 2, 2005; Revised Manuscript Received May 24, 2006

ABSTRACT: The accumulation of the cosolutes ethylene glycol, urea, glycine, sarcosine, and glycine betaine at the single-stranded DNA surface exposed upon melting the double helix has been quantified for DNA samples of different guanine−cytosine (GC) content using the local-bulk partitioning model [Record, M. T., Jr., Zhang, W., and Anderson, C. F. (1998) *Adv. Protein Chem. 51*, 281−353]. Urea and ethylene glycol are both locally accumulated at single-stranded DNA relative to bulk solution. Urea exhibits a stronger affinity for adenine (A) and thymine (T) bases, leading to a greater net dehydration of these bases upon DNA melting; ethylene glycol local accumulation is practically independent of base composition. However, glycine, sarcosine, and glycine betaine are not necessarily locally accumulated at single strands after melting relative to bulk solution, although they are locally accumulated relative to double-stranded DNA. The local accumulation of glycine, sarcosine, and glycine betaine at single strands relative to double-stranded DNA decreases with bulk cosolute molality and increases with GC content for all N-methylated glycines, demonstrating a stronger affinity for G and C bases. Glycine also shows a minimum in melting temperature T_m at 1−2 *m* for DNA samples of 50% GC content or less. Increasing ionic strength attenuates the local accumulation of urea, glycine, sarcosine, and glycine betaine and removes the minimum in T_m with glycine. This attenuation in local accumulation results in counterion release during the melting transition that is dependent on water activity and, hence, cosolute molality.

The double helix to single strand conformation equilibrium of DNA not only depends on base pairing and electrostatic interactions but also is sensitive to solvent composition. In aqueous solution at molar concentrations, uncharged cellular cosolutes such as polyhydric alcohols and sugars, amino acids, and N-methylated glycines all destabilize double-helical DNA, lowering both the melting temperature T_m of the duplex (*1*−*7*) and the enthalpy change of the duplex−single strand transition (*2*−*4*, *7*). To promote the transition from double helix to the single strand conformation, these cosolutes must interact favorably with, and accumulate at, the uncharged single-stranded DNA surface exposed during melting relative to double-stranded DNA (*8*, *9*). Indeed, any biochemical process that involves a change in the surface area of DNA may be sensitive to cosolute activity (*10*, *11*). For this reason, it is important to quantify the interaction of these uncharged cosolutes with DNA double- and single-stranded surfaces.

To date, the dependence of the DNA melting transition on cosolute concentration has been studied for a variety of cosolutes. Of interest to us are the N-methylated glycines glycine, sarcosine (*N*-methylglycine), *N*,*N*-dimethylglycine, and glycine betaine (*N*,*N*,*N*-trimethylglycine). These compounds form a homologous zwitterion series at neutral pH characterized by increasing hydrophobicity of the amine functional group. Duplex DNA thermal transition temperatures decrease approximately linearly with N-methylated glycine concentration (*4*, *5*). Rees et al. (*5*) observed that glycine betaine was an "isostabilizing" agent, eliminating the dependence of T_m on GC[1] composition. Specifically, the destabilizing effect of glycine betaine on DNA increases with increasing GC content with almost no effect on poly(dAdT). Barone et al. (*4*) demonstrated that the isostabilization capability of the N-methylated glycines increases with the number of methyl groups on the nitrogen atom; glycine betaine produces the greatest isostabilization effect followed by *N*,*N*-dimethylglycine, sarcosine, and glycine in that order. Glycine, sarcosine, and *N*,*N*-dimethylglycine produce only a modest reduction in the calorimetric enthalpy change (∼1 kcal/mol at ∼3 M) associated with the melting transition; however, the calorimetric enthalpy change for the melting transition is apparently unchanged in glycine betaine solutions (*4*).

Urea and ethylene glycol are also of interest because these cosolutes are potential hydrogen bond acceptors and donors

† This research was supported by an award from the Research Corporation (CC6299) and was also supported in part by a grant to St. Olaf College from the Howard Hughes Medical Institute through the Undergraduate Science Education Program.

* To whom correspondence should be addressed. Phone: (507) 646-3105. Fax: (507) 646-3968. E-mail: schwinef@stolaf.edu.

‡ St. Olaf College.

§ National Institutes of Health.

|| Washington University in St. Louis.

[1] Abbreviations: G, guanine; C, cytosine; A, adenine; T, thymine; ctDNA, calf thymus DNA.

10.1021/bi052469i CCC: $33.50
Published on Web 07/18/2006

but are significantly less polar than the zwitterionic N-methylated glycines. Both urea and ethylene glycol destabilize DNA (*1*, *7*, *12*, *13*), although unlike some proteins, DNA is intact even in 6 M aqueous urea solution (*7*, *12*, *13*). As with the N-methylated glycines, the enthalpy change associated with the thermal denaturation of DNA is reduced by approximately 1 kcal/mol in 3 M urea (*7*). However, in contrast to the N-methylated glycines, urea appears to destabilize AT base pairs more than GC base pairs (*12*).

Currently, quantitative thermodynamic measurements of cosolute−DNA interactions are only available for urea and glycine betaine with duplex DNA (*8*). Using vapor pressure osmometry and preferential interaction coefficients, Hong and co-workers observed that glycine betaine was strongly excluded from the double-helical DNA surface in aqueous KCl solutions, resulting in a preferential hydration of the DNA duplex (*8*). The exclusion of glycine betaine from the DNA surface was attributed to the preferential interaction of DNA and glycine betaine with water rather than each other. In contrast, urea is neither accumulated nor excluded from the vicinity of salt ions (K^+, Na^+, Cl^-) (*14*) and showed similar behavior near the anionic DNA surface; the local concentration of urea near DNA is essentially the same as that in bulk solution.

The local-bulk cosolute partitioning model of Record and co-workers (*8*, *9*, *15*) provides a thermodynamic model to quantify the preferential accumulation or exclusion of cosolutes from the DNA surface. The partitioning model interprets the accumulation or exclusion of cosolutes in terms of a local-bulk apparent partition coefficient, K_p. This apparent partition coefficient characterizes the partitioning of water and cosolute across a thermodynamic boundary defining a local domain near the DNA surface and bulk solution. The local domain is a potentially extensive region where the solvent is non-bulk-like, although in practice the local domain is marked by the first cosolute layer which may be within one or two hydration layers of the biopolymer surface (*16*). The local-bulk cosolute partitioning model has been used to interpret protein denaturation with guanidinium chloride and urea (*17*), the interactions of bovine serum albumin and hen egg lysozyme with glycine betaine and various other cosolutes (*18*, *19*), and the stabilization and denaturation of the lacI HTH DNA binding domain with glycine betaine and urea (*15*, *20*).

In the present study we quantify the melting of DNA of different base compositions in aqueous solutions of ethylene glycol, urea, glycine, sarcosine, and glycine betaine using the local-bulk partitioning model. We obtain a quantitative measure of the local concentration surplus of these cosolutes near the newly exposed DNA surface relative to double-stranded DNA for the melting transition, as well as the dependence of the apparent partition coefficient on cosolute concentration. Implications for cosolute interactions with DNA and hydration are discussed.

Background on Preferential Interactions and the Local-Bulk Partitioning Model. Consequences of accumulation or exclusion of uncharged cosolutes from duplex DNA on DNA conformational changes are best characterized by preferential interaction coefficients. Preferential interaction coefficients describe the effect of solute concentration on reactant and product macromolecule activity. For four-component solutions, such as dilute aqueous solutions of DNA (component 2) with fixed concentration of salt (component 4) and variable concentration of uncharged cosolute (component 3), the preferential interaction coefficient in the context of a dialysis experiment is given by (here component 1 is water) (*8*)

$$\Gamma_{\mu_3,m_4} = (\partial m_3/\partial m_2)_{T,P,\mu_3,m_4} \quad (1)$$

where m_i is the molality of species i and μ_3 is the chemical potential of cosolute. The thermodynamic expression for the dependence of the observed equilibrium constant K_{obs} for a biopolymer reaction (in our case DNA melting) on the activity of cosolute a_3 is

$$(\partial \ln K_{obs}/\partial \ln a_3)_{T,P,m_2,m_4} = \Delta\Gamma_{\mu_3,m_4} \quad (2)$$

where $\Delta\Gamma_{\mu_3,m_4}$ is the difference between values of Γ_{μ_3,m_4} characterizing interactions of cosolute with biopolymer products and reactants weighted by the stoichiometric coefficients in the biopolymer reaction equation (*8*, *9*, *21*, *22*). Wyman (*21*, *22*) demonstrated that eq 2 is independent of the way the reaction equation is formulated and that $\Delta\Gamma_{\mu_3,m_4}$ can be identified with the change in the amount of cosolute bound to the biopolymer during the course of the reaction. Values of $\Delta\Gamma_{\mu_3,m_4}$ are generally understood to represent the preferential interaction of cosolute with the biopolymer surface area newly exposed during the unfolding process (*17*). Positive values (negative values) of $\Delta\Gamma_{\mu_3,m_4}$ indicate that cosolute interaction is more thermodynamically favorable (unfavorable) with product than reactant, resulting in accumulation (exclusion) of cosolute at the newly exposed surface of the unfolded biopolymer.

For a cooperative biopolymer conformational change in a large excess of uncharged cosolute, the dependence of the observed equilibrium constant on cosolute activity (eq 2) can be related to the change in melting temperature T_m with cosolute activity a_3

$$\frac{dT_m^{-1}}{d \ln a_3} = \frac{R}{\Delta H^\circ_{T_m}} \Delta\Gamma_{\mu_3,m_4} \quad (3)$$

where R is the ideal gas constant and $\Delta H^\circ_{T_m}$ is the observed enthalpy change accompanying the unfolding process at T_m (*9*). With the Gibbs−Duhem relation (*23*), $d \ln a_3 = -(m_1^\bullet/m_3)(d \ln a_1)$ (assuming the salt is sufficiently dilute to have little effect on the activities of cosolute and water), where a_1 is the activity of water and $m_1^\bullet = 55.56$ mol kg^{-1} is the molality of water, eq 3 can be rewritten as

$$\frac{dT_m^{-1}}{d \ln a_1} = \frac{-Rm_1^\bullet}{\Delta H^\circ_{T_m}} \left(\frac{\Delta\Gamma_{\mu_3,m_4}}{m_3} \right) \quad (4)$$

Hence, $\Delta\Gamma_{\mu_3,m_4}$ can be related to the dependence of the melting temperature on either cosolute or water activity.

Record and co-workers (*8*, *15*, *17*−*20*) have developed a local-bulk cosolute partitioning model to interpret $\Delta\Gamma_{\mu_3,m_4}$ in terms of an apparent partition coefficient K_p that characterizes the concentration gradient of water and cosolute between the local domain near the biopolymer surface and bulk solution. Due to interactions of the biopolymer surface with uncharged cosolute, as well as the interactions of water with biopolymer and cosolute, the cosolute concentrations

in the local domain m_3^{local} and in the bulk domain m_3^{bulk} are expected to differ. For uncharged cosolutes, m_3^{local} and m_3^{bulk} are related to K_p by

$$K_p = \frac{m_3^{local}}{m_3^{bulk}} = \frac{(X_3/X_1)^{local}}{(X_3/X_1)^{bulk}} = \frac{(f_3/f_1)^{bulk}}{(f_3/f_1)^{local}} \quad (5)$$

where X_3 and X_1 are the mole fractions of cosolute and water, respectively, and f_3 and f_1 are the corresponding mole fraction activity coefficients. In the local-bulk cosolute partitioning model, $\Delta\Gamma_{\mu_3,m_4}$ is predicted to be proportional to ΔASA, the change in water-accessible surface area during the biopolymer unfolding transition (*8*, *15*, *17*−*20*)

$$\frac{\Delta\Gamma_{\mu_3,m_4}}{m_3^{bulk}} = \frac{(K_p - 1)b_1\Delta\text{ASA}}{m_1^\bullet} \quad (6)$$

In eq 6, b_1 is the amount of water in the local domain surrounding the biopolymer surface exposed during melting expressed as molecules of water per Å^2. Equation 6 demonstrates that K_p is associated with the surface area exposed upon unfolding, assuming the common surface area does not change. If cosolute is strongly accumulated or excluded from the biopolymer surface, the bulk concentration of cosolute, m_3^{bulk}, can be significantly different than m_3. However, in the dilute DNA solutions used in this work, m_3 is essentially m_3^{bulk} (*9*).

At low to moderate cosolute molality (0−1 *m*), $\Delta\Gamma_{\mu_3,m_4}$ is proportional to m_3^{bulk} if $K_p = K_p^o$ (here the superscript ° indicates a limiting value at low cosolute concentration) is concentration independent. This has been demonstrated for urea−KCl solutions (*14*) and a variety of protein−cosolute systems (*15*, *17*−*20*). However, the assumption of a concentration-independent K_p is not always valid, especially when cosolute thermodynamic nonideality has a strong dependence on cosolute concentration. As a result of the cosolute concentration gradient between the local and bulk domains and cosolute and water interactions with the biopolymer in the local domain, the nonideality of both water and cosolute may have different dependences on cosolute concentration in the two domains (*24*).

In the current work, we use the dependence of the DNA melting temperature on water activity to extract $\Delta\Gamma_{\mu_3,m_4}/m_3$ and K_p values for ethylene glycol, urea, glycine, sarcosine, and glycine betaine with DNA of different base composition. We also discuss the implications of cosolute interactions with the DNA helix on counterion and water release during the melting transition.

MATERIALS AND METHODS

Materials. *Clostridium perfringens*, calf thymus (ct), *Escherichia coli*, and *Micrococcus lysodeikticus* DNAs were purchased from Sigma Chemical Co. [Poly(dAdT)]$_2$ and [poly(dGdC)]$_2$ were purchased from Amersham. Glycine was obtained from Fisher, while sarcosine (*N*-methylglycine), glycine betaine (*N*,*N*,*N*-trimethylglycine), and urea were purchased from Sigma. Ethylene glycol was purchased from Eastman Organic Chemicals. All cosolutes were of reagent grade and were used without further purification. In our thermal melting studies, we used a 5 mM sodium phosphate and 0.1 mM Na_2EDTA buffer, pH 6.9 (8 m*m* Na^+). Phosphate buffer components $NaH_2PO_4{\cdot}H_2O$, Na_2HPO_4, and Na_2EDTA were all purchased from Fisher Scientific.

Table 1: Nucleic Acid Samples Used in Melting Experiments

nucleic acid	% GC	ϵ/M^{-1} cm^{-1} [a]	$\Delta H°_{T_m}$/kcal mol^{-1} (base pair)$^{-1}$
[poly(dAdT)]$_2$	0	13200[b]	8.06[d]
C. perfringens	31	12476[b]	8.55[e]
calf thymus	42	12824[b]	7.74[f]
			8.26[g]
			8.81[h]
E. coli	50	13080[c]	7.70[i]
M. lysodeikticus	72	13846[b]	8.89[e]
[poly(dGdC)]$_2$	100	16800[b]	12.10[d]

[a] Per base pair; λ = 260 nm for natural DNAs, λ = 254 nm for [poly(dAdT)]$_2$, and λ = 262 nm for [poly(dGdC)]$_2$. [b] From Chaires et al. (*25*). [c] From Chalikian et al. (*26*). [d] From Chalikian et al. (*33*), 32 mM Na^+ buffer. [e] Extrapolated from enthalpy data in Karapetian et al. (*34*) to 8 m*m* Na^+. [f] Extrapolated from enthalpy data in Gruenwedel (*35*) to 8 m*m* Na^+. [g] Interpolated from enthalpy data in Gruenwedel (*35*) at 58 m*m* Na^+. [h] Interpolated from enthalpy data in Gruenwedel (*35*) at 158 m*m* Na^+. [i] From Spink and Chaires (*1*).

Lyophilized DNA samples were suspended at 0.5−1 mg/mL in a 100 mM NaCl and 5 mM sodium phosphate, pH 6.9, solution, dialyzed exhaustively versus 5 mM sodium phosphate buffer, and stored at 4 °C. DNA concentrations were determined by absorbance at 260 nm using appropriate extinction coefficients (*25*, *26*) (see Table 1).

DNA Melts. Buffers were prepared gravimetrically to determine both the molarity and molality of buffer components. The pH of all cosolute solutions was within 0.4 pH unit of pH 6.9. All buffers were used within 3 days of preparation. DNA−cosolute solutions were prepared gravimetrically by mixing the stock DNA solution, cosolute, sodium phosphate buffer, and a stock 1 *m* NaCl solution. Final NaCl concentrations were 0, 50, or 150 m*m*. Gravimetric preparation of the solutions ensured constant DNA and Na^+ molality with varying cosolute molality. Solutions were degassed with nitrogen prior to melting. DNA thermal transitions were monitored at 260 nm using a Cary 100 UV−visible spectrophotometer (Varian) equipped with a Peltier temperature controller. Teflon-stoppered quartz cuvettes from Fisher Scientific with a 1 cm path length were used. DNA samples were heated at a rate of 0.4 °C/min, and absorbance readings were collected every 0.5 °C. Double-stranded and melted DNA plateau regions in the absorbance melting profiles were fit by linear regression; the fraction of DNA melted in the sample was determined from the difference in absorbance between our experimentally measured values and the extrapolated fits. The T_m was identified with the transition midpoint (50% DNA melted) for each DNA sample. The uncertainty in T_m was ±0.1 °C.

Application of the Local-Bulk Partitioning Model to DNA Melting Data. Evaluation of $\Delta\Gamma_{\mu_3,m_4}/m_3$ and the apparent partition coefficient K_p in eqs 4 and 6 requires knowledge of the water mole fraction activity a_1. Water activities were determined from osmotic coefficients ϕ (*27*) using the relation osmolality $\equiv \phi m_3 = -m_1^\bullet \ln a_1$ for ethylene glycol (*28*), urea (*29*), glycine (*30*, *31*), sarcosine (*32*), and glycine betaine (*32*) solutions. Water activities were not corrected for the 5 mM sodium phosphate and 0.1 mM Na_2EDTA buffer components. However, for those DNA melting experi-

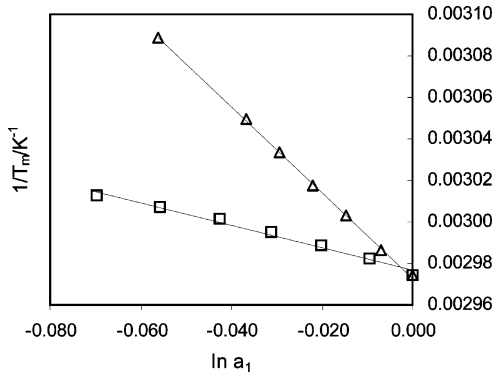

FIGURE 1: Inverse melting temperature, T_m^{-1}, as a function of the natural logarithm of water activity (ln a_1) for ctDNA with ethylene glycol (□) and urea (△) in 5 mM sodium phosphate buffer.

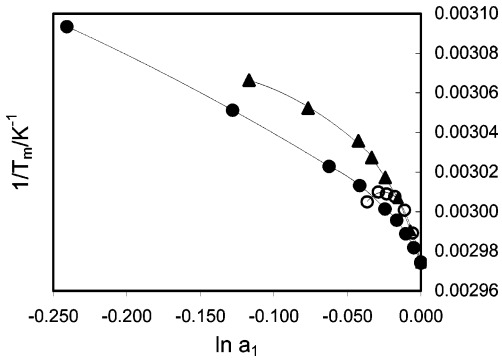

FIGURE 2: Inverse melting temperature, T_m^{-1}, as a function of the natural logarithm of water activity (ln a_1) for ctDNA with glycine (○), sarcosine (▲), and glycine betaine (●). Lines are included to indicate trends. Buffer conditions as in Figure 1.

ments with added NaCl (50 and 150 m*m*), water activities were determined from the sum of NaCl and cosolute osmolalities. The osmolalities of KCl and urea and of KCl and glycine betaine have been shown to be additive (*8*, *14*). Using a Wescor vapor pressure osmometer (model 5520), we have verified that the osmolality of NaCl and the osmolality of either ethylene glycol, urea, glycine, sarcosine, or glycine betaine are additive up to ~2 *m* cosolute (the maximum cosolute concentration for our Wescor osmometer). We made no temperature correction for water activity in our analysis.

Enthalpy changes for the DNA melting transition were obtained from DNA thermal denaturation data in Na^+ solutions and are tabulated in Table 1. For $[poly(dGdC)]_2$ and $[poly(dAdT)]_2$ melts in 5 mM sodium phosphate buffer, we use $\Delta H°_{T_m}$ values at 32 mM Na^+ (*33*) assuming minimal change in $\Delta H°_{T_m}$ over this Na^+ concentration range (*34*, *35*). For the natural DNA samples used in this study, DNA melting enthalpies were obtained by interpolating or extrapolating published enthalpy values to our Na^+ concentrations of interest (*1*, *34*, *35*). In determining $\Delta\Gamma_{\mu_3,m_4}/m_3$ from eq 4, we use $\Delta H°_{T_m}$ for cosolute-free solutions since $\Delta H°_{T_m}$ shows only a small dependence on cosolute concentration at our cosolute concentrations of interest (*2*, *4*, *7*).

Since T_m^{-1} is a linear function of ln a_1 (Figure 1) for all DNA samples in ethylene glycol and urea solutions, values of $\Delta\Gamma_{\mu_3,m_4}/m_3$ and associated errors were determined from linear regression. However, for the N-methylated glycines with all DNA samples, T_m^{-1} is not linear with ln a_1 (Figure 2). Since multiple linear regression of T_m^{-1} with ln a_1 introduces artifacts in $dT_m^{-1}/(d \ln a_1)$, $dT_m^{-1}/(d \ln a_1)$ was determined as follows for DNA melts in N-methylated glycine solutions. The slope $dT_m^{-1}/(d \ln a_1)$ at the *i*th data point in a plot of T_m^{-1} versus ln a_1 was calculated by averaging the slopes between the data points $i - 1$ and i and i and $i + 1$. Slopes at the initial and final data points were determined using that data point and its nearest neighbor. Propagation of error was used to determine the standard error in $dT_m^{-1}/(d \ln a_1)$ assuming the uncertainty in T_m was ±0.1 °C.

To extract the apparent partition coefficient K_p from $\Delta\Gamma_{\mu_3,m_4}/m_3$ in eq 6 at each cosolute concentration and for each DNA sample, we used $b_1 = 0.11$ $H_2O/Å^2$ and ΔASA = 200 $Å^2$/base pair (*8*). This change in solvent-accessible surface area assumes half-stacking of nucleotides in the single strand, relative to the conformation of nucleotides in the double helix. Hong et al. (*8*) have shown the change in solvent-accessible surface area to be practically independent of GC content.

RESULTS

Effect of Ethylene Glycol and Urea on DNA Melting. As previously noted, both ethylene glycol and urea destabilize DNA (*1*, *7*, *12*, *13*) so that increasing ethylene glycol and urea concentrations progressively lower DNA melting temperatures. For each DNA sample studied, T_m^{-1} decreases linearly with increasing water activity (decreasing ethylene glycol and urea molality) (Figure 1). Linear regression of T_m^{-1} as a function of ln a_1 yields concentration-independent $\Delta\Gamma_{\mu_3,m_4}/m_3$ and K_p values (eqs 4 and 6) for each DNA sample (Table 2). In all cases, $\Delta\Gamma_{\mu_3,m_4}/m_3$ is positive and K_p is >1, indicating a greater accumulation of ethylene glycol and urea at the newly exposed surface of melted DNA relative to double-stranded DNA.

Hong et al. (*8*) have demonstrated that urea is randomly distributed between the local and bulk domains of double-stranded ctDNA, independent of urea molality, with $\Gamma_{\mu_3,m_4}/m_3 \approx 0$. Hultgren and Rau (*36*) have also measured little inclusion or exclusion of glycerol around spermidine^{3+}–DNA condensed arrays. Therefore, we also anticipate the homologous compound ethylene glycol to be neither preferentially accumulated nor excluded from the local domain of double-stranded DNA. Given the observed DNA melting reaction where S_1 and S_2 represent the single strands in the DNA helix

$$S_1S_2 \rightleftarrows S_1 + S_2 \tag{7}$$

we can write

$$\Delta\Gamma_{\mu_3,m_4}/m_3 = (\Gamma_{\mu_3,m_4}/m_3)_{S_1} + (\Gamma_{\mu_3,m_4}/m_3)_{S_2} - (\Gamma_{\mu_3,m_4}/m_3)_{S_1S_2} \tag{8}$$

Since we anticipate $(\Gamma_{\mu_3,m_4}/m_3)_{S_1S_2} \approx 0$ for ethylene glycol and urea, our $\Delta\Gamma_{\mu_3,m_4}/m_3$ (and K_p) values are a measure of both favorable interaction and accumulation of these cosolutes near the surface of single-stranded DNA.

The K_p values in Table 2 are smaller for ethylene glycol than urea, indicating that T_m^{-1} has a stronger dependence on urea concentration for all of the DNA samples studied. The ethylene glycol K_p values are 1.10–1.17, suggesting a 10–17% higher concentration of ethylene glycol at the newly

Table 2: $\Delta\Gamma_{\mu_3,m_4}/m_3$ and K_p Values in Ethylene Glycol and Urea Solutions[a]

		ethylene glycol		urea	
	NaCl/m*m*	$\Delta\Gamma_{\mu_3,m_4}/m_3/m^{-1}$ [b]	K_p	$\Delta\Gamma_{\mu_3,m_4}/m_3/m^{-1}$ [b]	K_p
[poly(dAdT)]$_2$	0	0.056 ± 0.003	1.14 ± 0.01	0.203 ± 0.007	1.51 ± 0.02
C. perfringens	0	0.046 ± 0.002	1.12 ± 0.01	0.171 ± 0.001	1.43 ± 0.01
calf thymus	0	0.038 ± 0.002	1.10 ± 0.01	0.144 ± 0.001	1.36 ± 0.01
	50	0.053 ± 0.002	1.13 ± 0.01	0.109 ± 0.002	1.28 ± 0.01
	150	0.058 ± 0.002	1.15 ± 0.01	0.089 ± 0.005	1.23 ± 0.01
E. coli	0	0.045 ± 0.002	1.11 ± 0.01	0.126 ± 0.003	1.32 ± 0.01
M. lysodeikticus	0	0.053 ± 0.002	1.14 ± 0.01	0.093 ± 0.010	1.24 ± 0.02
[poly(dGdC)]$_2$	0	0.068 ± 0.003	1.17 ± 0.01		

[a] All DNA−cosolute solutions were prepared in 5 mM sodium phosphate and 0.1 mM Na_2EDTA buffer. [b] Per DNA base pair.

exposed DNA surface relative to bulk solution. Larger K_p values for urea signal markedly greater accumulation of urea at the DNA surface exposed upon melting. Although values of K_p are nearly independent of GC content for ethylene glycol, these values mirror the dependence of $\Delta H^\circ_{T_m}$ on GC content (Table 1). In this case, both low and high GC content ([poly(dAdT)]$_2$, [poly(dGdC)]$_2$) correspond to the largest K_p values, while ctDNA and *E. coli* DNA with mixed base composition exhibit the smallest K_p values.

Increasing DNA GC content corresponds to decreasing K_p values for urea. Babayan (*12*) observed a greater decrease in the thermostability of AT base pairs than GC base pairs with urea, which we also observe. That is, larger K_p values calculated for AT-rich DNA indicate greater accumulation of urea at A and T bases exposed after melting and, thus, greater destabilization of AT base pairs. It is also noteworthy that, as AT or GC content of DNA increases (i.e., as base composition becomes more homogeneous), hydration of the double helix increases (*26*). Because of its strong hydrogen-bonding capacity, urea can compete with water for hydrogen-bonding sites along DNA. Although Hong et al. (*8*) demonstrated that urea is neither accumulated nor excluded from the surface of the ctDNA double helix, higher accumulation of urea occurs at A and T bases exposed upon DNA melting than at newly exposed G and C bases, presumably due to more efficient dehydration of A and T bases (see Discussion).

Effect of Glycine, Sarcosine, and Betaine on DNA Melting. Unlike ethylene glycol and urea, plots of T_m^{-1} versus ln a_1 for the N-methylated glycines in 5 mM phosphate buffer exhibit notable concave-downward curvature for all DNA samples studied. A representative plot of T_m^{-1} versus ln a_1 for ctDNA is shown in Figure 2. These nonlinear plots indicate concentration-dependent $\Delta\Gamma_{\mu_3,m_4}/m_3$ and K_p values, possibly due to the nonideality of water, salt, and cosolute in the local domain of DNA (*15*).

Values of $\Delta\Gamma_{\mu_3,m_4}/m_3$ and the apparent partition coefficient K_p for the N-methylated glycines are shown in Figures 3 and 4, respectively, as functions of m_3 for all DNA samples studied. In all cases, as indicated by the concave-down curvature of the curves in Figure 2, $\Delta\Gamma_{\mu_3,m_4}/m_3$ and K_p are decreasing functions of m_3. Initial values of $\Delta\Gamma_{\mu_3,m_4}/m_3$, $\Delta\Gamma^\circ_{\mu_3,m_4}/m_3$, and K_p, K_p^o, for a given DNA GC content, as well as $\Delta\Gamma_{\mu_3,m_4}/m_3$ and K_p at any m_3, decrease with the addition of *N*-methyl groups; that is, $\Delta\Gamma^\circ_{\mu_3,m_4}/m_3$ and K_p^o for glycine are greater than $\Delta\Gamma^\circ_{\mu_3,m_4}/m_3$ and K_p^o for sarcosine, which are greater than those for glycine betaine for all DNA samples studied. This indicates less accumulation of N-methylated glycine at the newly exposed single-stranded DNA surface with increasing methylation of the glycine amine functional group. This trend may be attributed in part to glycine's capacity to form several strong hydrogen bonds with the bases exposed upon DNA melting. Glycine and sarcosine can both accept and donate hydrogen bonds, whereas glycine betaine can only accept hydrogen bonds and, significantly, has the smallest $\Delta\Gamma^\circ_{\mu_3,m_4}/m_3$ and K_p^o values of the N-methylated glycines. However, this does raise the question why the N-methylated glycine−DNA interaction does not look more like traditional binding (T_m^{-1} linear with ln a_3). In addition, the reduction in the accumulation of N-methylated glycines with the addition of *N*-methyl moieties may also be due to increasingly unfavorable interactions of the progressively more hydrophobic amine functional group with the negatively charged DNA backbone and newly exposed hydrogen-bonding bases (see Discussion). Notably,

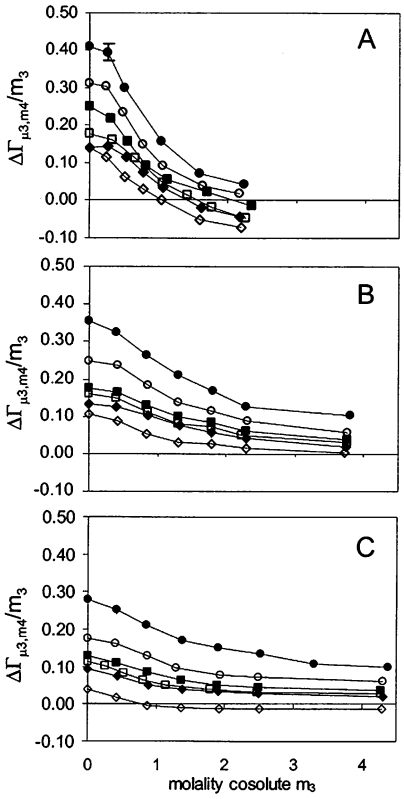

FIGURE 3: Change in preferential cosolute interaction parameter, $\Delta\Gamma_{\mu_3,m_4}/m_3$, with (A) glycine, (B) sarcosine, and (C) glycine betaine molality for [poly(dAdT)]$_2$ (◇), *C. perfringens* (◆), ctDNA (□), *E. coli* (■), *M. lysodeikticus* (○), and [poly(dGdC)]$_2$ (●). Magnitude of standard error indicated on a single point in (A). Buffer conditions as in Figure 1.

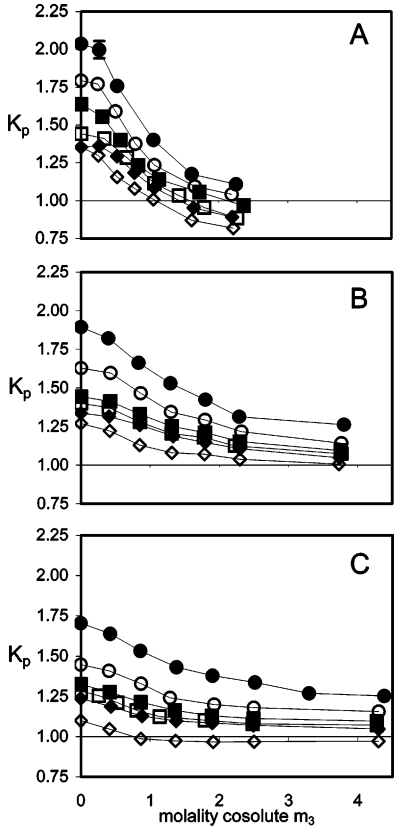

FIGURE 4: Dependence of K_p on (A) glycine, (B) sarcosine, and (C) glycine betaine molality for [poly(dAdT)]$_2$ (◇), *C. perfringens* (◆), ctDNA (□), *E. coli* (■), *M. lysodeikticus* (○), and [poly(dGdC)]$_2$ (●). Magnitude of standard error indicated on a single point in (A). Buffer conditions as in Figure 1.

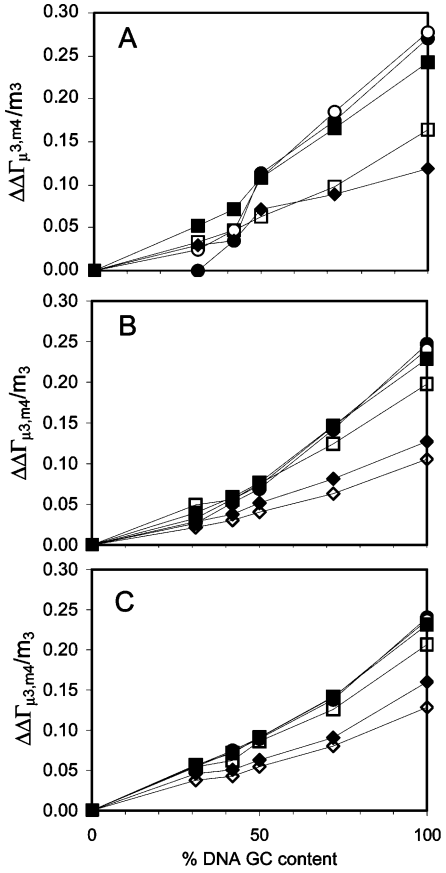

FIGURE 5: Comparison of $\Delta\Delta\Gamma_{\mu_3,m_4}/m_3$, the change in preferential cosolute interaction parameter relative to [poly(dAdT)]$_2$, as a function of % GC content at 0 (●), 0.25 (○), 0.50 (■), 1.00 (□), 2.00 (◆), and 3.00 *m* (◇) cosolute. Plots: (A) glycine, (B) sarcosine, and (C) glycine betaine. Buffer conditions as in Figure 1.

K_p^o values in Figure 4 for glycine are much larger than the m_3-independent K_p values for urea and ethylene glycol (Table 2), indicating a stronger interaction of glycine with the newly exposed DNA surface relative to double-stranded DNA at low m_3.

Hong et al. (*8*) have demonstrated that glycine betaine is strongly excluded from the vicinity of double-stranded ctDNA, with $\Gamma_{\mu_3,m_4}/m_3 = -0.6$ (per base pair) in 200−400 m*m* KCl, independent of glycine betaine molality. Using the limiting value $\Delta\Gamma^\circ_{\mu_3,m_4}/m_3 = 0.13$ from Figure 3 for ctDNA and glycine betaine and using eqs 7 and 8, we estimate $(\Gamma_{\mu_3,m_4}/m_3)^o_S = -0.24$ for ctDNA single strands (assuming $\Gamma_{\mu_3,m_4}/m_3$ is the same for either strand and $\Gamma_{\mu_3,m_4}/m_3 = -0.6$ is valid in our 5 mM phosphate buffer). Thus, glycine betaine is still excluded from ctDNA single strands, and our values of $\Delta\Gamma_{\mu_3,m_4}/m_3$ indicate greater accumulation of glycine betaine around single strands only relative to double-stranded DNA. In addition, $\Delta\Gamma_{\mu_3,m_4}/m_3$ decreases with glycine betaine molality (Figure 3). Therefore, $(\Gamma_{\mu_3,m_4}/m_3)_S$ must also become more negative with glycine betaine molality, indicating greater exclusion of glycine betaine from single strands with increasing molality of cosolute. The reason for the decrease in glycine betaine exclusion around single strands relative to double-stranded DNA is unclear. It is reasonable that the decrease in exclusion is due purely to local accumulation of glycine betaine near bases exposed upon melting. It is also possible, however, that the water organized by DNA bases in the major and minor grooves of the double helix excludes glycine betaine in a sequence-dependent manner and that this exclusion disappears with melting and the loss of grooves. Unfortunately, preferential interaction parameters have not been measured for glycine or sarcosine with double-stranded DNA. We can conclude, however, that our measured values of $\Delta\Gamma_{\mu_3,m_4}/m_3$ and K_p do not necessarily indicate local accumulation of these cosolutes at single strands but, instead, indicate, at least, a reduction in local exclusion of the N-methylated glycines at single strands relative to double-stranded DNA.

For the N-methylated glycines at all cosolute concentrations, $\Delta\Gamma_{\mu_3,m_4}/m_3$ (Figure 3) and K_p (Figure 4) increase with increasing GC content of DNA, opposite to that observed with urea. Increased interaction of the N-methylated glycines with G and C bases may be explained by the additional opportunity for hydrogen bond formation offered by G and C bases as compared to A and T bases. The isostabilizing effect of the N-methylated glycines (*4*, *5*) is quantified by these trends in $\Delta\Gamma_{\mu_3,m_4}/m_3$ and K_p, with glycine betaine producing a minimal impact on [poly(dAdT)]$_2$ melting temperatures ($\Delta\Gamma_{\mu_3,m_4}/m_3 \approx 0$ and $K_p \approx 1$ at all m_3).

To understand the enhanced local accumulation of the N-methylated glycines around DNA single strands with increasing GC content, we determined the difference $\Delta\Delta\Gamma_{\mu_3,m_4}/m_3 = (\Delta\Gamma_{\mu_3,m_4}/m_3)_i - (\Delta\Gamma_{\mu_3,m_4}/m_3)_{[poly(dAdT)]_2}$ (where *i* represents a DNA sample with a given GC content) for each N-methylated glycine by interpolating the plots in Figure 3. Figure 5 plots $\Delta\Delta\Gamma_{\mu_3,m_4}/m_3$ as a function of GC content at 0, 0.25, 0.50, 1.0, 2.0, and 3.0 *m* N-methylated glycine. For all

the N-methylated glycines, $\Delta\Delta\Gamma_{\mu_3,m_4}/m_3$ values have similar magnitudes at the same molality. For example, at 0.50 *m* and 100% GC content, $\Delta\Delta\Gamma_{\mu_3,m_4}/m_3 = 0.24$ for glycine, 0.23 for sarcosine, and 0.23 for glycine betaine. Assuming the interaction of the N-methylated glycines with the phosphate backbone is the same in $[poly(dAdT)]_2$ as it is in DNA of higher GC content, this enhanced accumulation of the N-methylated glycines with increasing GC content must represent enhanced accumulation around the bases apart from the DNA backbone. It is unclear if the enhanced accumulation of the N-methylated glycines occurs at nucleotide regions previously secluded within the double helix and exposed upon melting or at nucleotide regions in the major and minor grooves of DNA that are exposed upon loss of hydrating waters. However, the near equivalent accumulation of the N-methylated glycines at GC-containing single-stranded DNA relative to $[poly(dAdT)]_2$ may represent hydrogen bonding between the anionic carboxylate of glycine, sarcosine, and glycine betaine with exposed bases. If the amine functional group were strongly involved in the interaction with exposed bases, the local accumulation of the N-methylated glycines relative to $[poly(dAdT)]_2$ would be expected to be radically different given the difference in the number of methyl moieties for the N-methylated glycines. In Figure 5, $\Delta\Delta\Gamma_{\mu_3,m_4}/m_3$ for glycine with GC-rich DNA is slightly larger than that for sarcosine and glycine betaine; this difference could represent some additional interaction of the amine functional group in glycine with the exposed bases, different than that for sarcosine or glycine betaine.

In Figure 2, T_m^{-1} achieves a maximum at $\ln a_1 \approx -0.025$ for ctDNA in a 1.6 *m* glycine solution. This maximum in T_m^{-1} for ctDNA is represented in Figures 3 and 4 where $\Delta\Gamma_{\mu_3,m_4}/m_3$ intersects zero and K_p intersects unity, respectively (see eqs 4 and 6). Figures 3 and 4 also indicate, as with ctDNA, DNA with a GC content of 50% or less achieves a maximum in T_m^{-1} at 1−2 *m* glycine (where $\Delta\Gamma_{\mu_3,m_4}/m_3$ intersects zero and K_p intersects one). This maximum in T_m^{-1} shifts to lower glycine concentration with increasing AT content. The maximum in T_m^{-1} corresponds to $\Delta\Gamma_{\mu_3,m_4}/m_3$ becoming negative in Figure 3, indicating a transition from less exclusion of glycine in the local domain surrounding the two single strands of DNA to more exclusion relative to double-stranded DNA.

However, there is evidence for a perturbation of B-DNA double helix structure with added glycine. Flock and co-workers (*37*, *38*) have shown that the circular dichroism spectra of calf thymus, $[poly(dAdT)]_2$, and $[poly(dGdC)]_2$ DNA in 1.5 M glycine all have a 20% reduction in intensity at 275 nm in 1 mM cacodylate buffer. This reduction in intensity has been attributed to a decrease in hydration of the DNA double helix leading to a perturbation of DNA double helix structure (*39*, *40*). If a DNA double helix structural change is responsible for maxima in T_m^{-1}, it only manifests for DNA GC content of 50% or less. Indeed, Chalikian et al. (*26*) has proposed that water molecules hydrating AT base pairs are less compact than are water molecules hydrating GC base pairs, reflective of weaker AT-rich DNA−water interactions. Thus, we propose that the maximum in T_m^{-1} is determined by a greater dehydration of AT-rich double-helical DNA with any concomitant structural change, despite the preference of glycine for G and C bases, quantified by larger $\Delta\Gamma_{\mu_3,m_4}/m_3$ and K_p values for GC-rich DNA (Figures 3 and 4). Modification of hydration patterns on AT-rich DNA may lead to changes in our local-bulk domain parameters ΔASA and b_1. However, we do not incorporate any potential changes in helical and hydration structure due to glycine; that is, we use values of ΔASA and b_1 for DNA samples in glycine-free solutions.

A minimum in T_m with glycine concentration is not consistently reported in the literature. Using absorbance spectroscopy at 260 nm, Rajendrakumar and co-workers (*41*) have shown the melting temperature of ctDNA in a 10 mM Tris-HCl buffer with 2 M glycine to be larger than that without any added glycine. However, Barone et al. (*4*) observed no minimum in T_m for ctDNA using differential scanning calorimetry in a 1 mM Tris buffer with 10 mM NaCl. We also see, as explained in the next section, that with added salt the maximum in T_m^{-1} in DNA−glycine solutions vanishes, potentially reconciling the observations of Rajendrakumar et al. (*41*) and Barone et al. (*4*).

The minimum in T_m for DNA of 50% GC content or less in glycine solutions is contrary to protein unfolding in the presence of glycine betaine. Unlike the enhanced accumulation of glycine in the local domain of DNA single strands relative to double strands, glycine betaine is excluded from the local domain of proteins, enhancing the stability of the proteins and increasing T_m (*42*). A maximum in T_m is observed for RNase and lysozyme (*43*) with added glycine betaine due to glycine betaine−glycine betaine interactions becoming more unfavorable in bulk solution relative to the local domain (*15*). The local-bulk domain model has been used to successfully interpret this behavior in proteins (*15*), and it predicts that glycine−glycine interactions become more favorable in the bulk solution than in the DNA local domain, leading to a minimum in T_m, assuming any structural change in double-helical DNA with added glycine has little impact on the model parameters $\Delta H^\circ_{T_m}$, ΔASA, and b_1.

Addition of NaCl Reduces the Dependence of $\Delta\Gamma_{\mu_3,m_4}/m_3$ *on* m_3. Addition of NaCl results in a slight decrease in $\Delta\Gamma_{\mu_3,m_4}/m_3$ and K_p for solutions of ctDNA and urea as reported in Table 2. This indicates a slight decrease in the accumulation of urea at the newly exposed DNA surface with increasing NaCl molality. Values of $\Delta\Gamma_{\mu_3,m_4}/m_3$ and K_p for ethylene glycol and ctDNA actually increase slightly with NaCl molality. Both the specific nature of the cosolute and salt concentration could perturb the conformation of single strands. However, in our analysis, we consider ΔASA to be salt and cosolute independent.

As representative plots, Figure 6 illustrates the increasingly linear dependence of ctDNA T_m^{-1} on $\ln a_1$ with NaCl molality for glycine, sarcosine, and glycine betaine. Except for the special case of ctDNA melts in glycine solutions with no added NaCl, as the ionic strength increases, $dT_m^{-1}/(d \ln a_1)$ decreases. That is, $\Delta\Gamma_{\mu_3,m_4}/m_3$ decreases at a given m_3 (Figure 7) with increasing ionic strength, indicating an increase in the local exclusion of N-methylated glycines at single strands. As seen in Figure 7, values of $\Delta\Gamma_{\mu_3,m_4}/m_3$ at 50 m*m* NaCl are only slightly greater, and nearly indistinguishable given experimental errors, than those at 150 m*m* for all of the N-methylated glycines.

Again, we can use the value $\Gamma_{\mu_3,m_4}/m_3 = -0.6$ (per base pair) in 200−400 m*m* KCl for ctDNA in aqueous glycine betaine solutions (*8*) to estimate the local exclusion of glycine betaine from ctDNA single strands. Using the limiting value

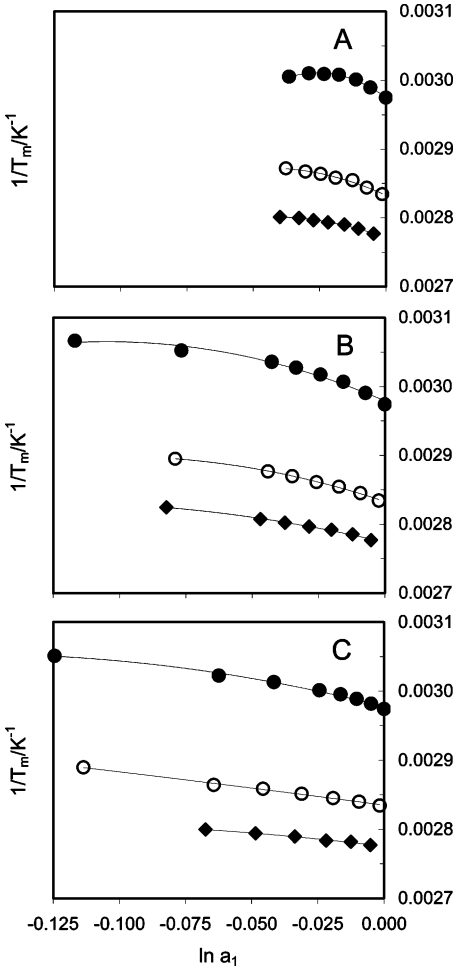

FIGURE 6: Calf thymus DNA inverse melting temperature, T_m^{-1}, as a function of the natural logarithm of water activity (ln a_1) for (A) glycine, (B) sarcosine, and (C) glycine betaine with 0 *m* (●), 50 m*m* (○), and 150 m*m* (◆) NaCl. Lines are drawn to indicate trends. Buffer conditions as in Figure 1.

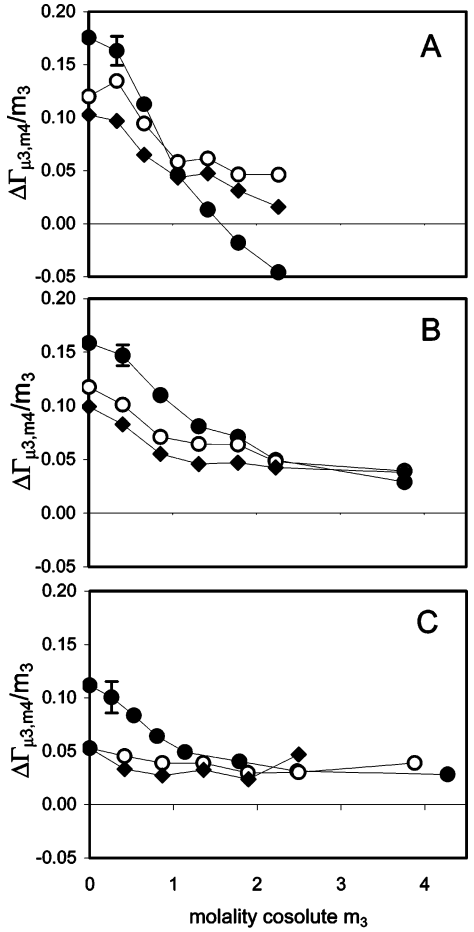

FIGURE 7: Change in preferential cosolute interaction parameter, $\Delta\Gamma_{\mu_3,m_4}/m_3$, with cosolute molality for (A) glycine, (B) sarcosine, and (C) glycine betaine with 0 *m* (●), 50 m*m* (○), and 150 m*m* (◆) NaCl. Magnitude of standard error indicated on a single point in each panel. Buffer conditions as in Figure 1.

$\Delta\Gamma^{\circ}_{\mu_3,m_4}/m_3 = 0.053$ from Figure 7 for ctDNA and glycine betaine at 50 and 150 m*m* NaCl and using eqs 7 and 8, we estimate $(\Gamma_{\mu_3,m_4}/m_3)^0_S = -0.27$ for ctDNA single strands (assuming $\Gamma_{\mu_3,m_4}/m_3$ is the same for either strand).

The T_m^{-1} maximum observed for ctDNA melts in glycine solutions vanishes in 50 m*m* NaCl. In Figure 7, $\Delta\Gamma_{\mu_3,m_4}/m_3$ is greater than zero with added NaCl, indicating local glycine accumulation at the newly exposed ctDNA surface relative to double-stranded DNA for all glycine molalities with no evidence of any potential DNA structural change.

DISCUSSION

Counterion Release during the DNA Melting Transition in Cosolute Solutions. At 50 m*m* NaCl, T_m^{-1} for ctDNA becomes nearly linear in glycine, sarcosine, and glycine betaine molality (Figure 6). Within the framework of the local-bulk domain model, the nonideality of the N-methylated glycines in the local domain approaches that of the bulk domain as the ionic strength increases (*15*). Additionally, $\Delta\Gamma_{\mu_3,m_4}/m_3$ decreases for urea and the N-methylated glycines and increases slightly for ethylene glycol (Table 2, Figure 7) with increasing ionic strength. Also, the maximum in ctDNA T_m^{-1} with glycine vanishes at 50 m*m* NaCl, reflective of reduced accumulation of glycine at the newly exposed DNA surface (Figures 6 and 7). Hence, NaCl must attenuate interactions between the newly exposed DNA surface and cosolutes.

The reduction of $dT_m^{-1}/(d \ln a_1)$ with increasing NaCl molality in Figure 6, mirrored by the reduced dependence of $\Delta\Gamma_{\mu_3,m_4}/m_3$ on m_3 at 50 and 150 m*m* NaCl (Figure 7), suggests that the number of condensed counterions released to the counterion atmosphere during the ctDNA melting transition is dependent on water activity (and hence, cosolute molality). The number of sodium ions released in the melting transition Δn_{Na^+} can be determined from (*44*)

$$-\frac{\Delta H^{\circ}_{T_m}}{R}\left(\frac{dT_m^{-1}}{d \ln m_{Na^+}}\right) = \alpha\frac{\Delta n_{Na^+}}{2} \qquad (9)$$

where α accounts for the nonideality of the monovalent ions and is approximately 0.9 in our case (*44*). For each of our different NaCl concentrations (0, 50, and 150 m*m*), we interpolated T_m^{-1} from our plots in Figure 6 (as well as those for urea and ethylene glycol) at water activities of ln $a_1 = -0.005$, -0.010, -0.020, and -0.030. Linear regression of T_m^{-1} versus ln m_{Na^+} (where $m_{Na^+} = 8$, 58, and 158 m*m*) at a given water activity was used to determine Δn_{Na^+} (per phosphate) in Table 3 as a function of water activity for each of the cosolutes studied in this work. The values of Δn_{Na^+} in Table 3 are of similar magnitude with those for ctDNA

Table 3: Number of Na^+ Ions Δn_{Na^+} Released per DNA Phosphate in Ethylene Glycol, Urea, and N-Methylated Glycine Solutions[a]

	Δn_{Na^+}				
ln a_1	ethylene glycol	urea	glycine	sarcosine	betaine
0.000[b]	0.30 ± 0.01	0.30 ± 0.02	0.30 ± 0.01	0.30 ± 0.01	0.30 ± 0.01
−0.005	0.30 ± 0.01	0.30 ± 0.02	0.31 ± 0.01	0.31 ± 0.01	0.31 ± 0.02
−0.010	0.30 ± 0.01	0.31 ± 0.02	0.32 ± 0.01	0.32 ± 0.01	0.31 ± 0.02
−0.020	0.29 ± 0.01	0.32 ± 0.02	0.32 ± 0.01	0.33 ± 0.02	0.32 ± 0.02
−0.030	0.29 ± 0.01	0.34 ± 0.02	0.31 ± 0.01	0.34 ± 0.01	0.32 ± 0.02

[a] All DNA−cosolute solutions were prepared in 5 mM sodium phosphate and 0.1 mM Na_2EDTA buffer (8 m*m* Na^+) with 0, 50, or 150 m*m* NaCl. [b] Water activity in the absence of cosolute and neglecting contribution from phosphate buffer and NaCl.

determined in earlier studies using ethylene glycol (*1*) and arabitol (*2*) as cosolutes.

For all cosolutes studied, Δn_{Na^+} is dependent on water activity (and thus m_3). This dependence on water activity is more pronounced for cosolutes more polar than water, namely, urea and the N-methylated glycines (*45*). The stoichiometric release of sodium ions is largest at ln $a_1 = -0.030$ for urea and sarcosine. The increase and then decrease in Δn_{Na^+} with ln a_1 for glycine is due to the presence of a maximum in T_m^{-1} with water activity with no added NaCl (Figures 2 and 6). However, before decreasing at ln $a_1 = -0.10$, Δn_{Na^+} in aqueous glycine solutions has the same value as that in sarcosine solutions. Of the N-methylated glycines, glycine betaine has the weakest dependence of Δn_{Na^+} on water activity; this could in part be due to an attenuation of any competition of the N-methylated glycines with sodium ions for DNA phosphates as the number of methyl moieties increases on the positively charged amine.

However, Δn_{Na^+} also increases in aqueous urea solutions and decreases in aqueous ethylene glycol solutions. The N-methylated glycines and urea are more polar than water and increase the solution dielectric constant while ethylene glycol decreases the dielectric constant (*45*). As the bulk concentration of cosolute is increased, the local concentration at double-stranded and single-stranded DNA must also increase, although the extent of the increase is dependent on the level of accumulation or exclusion from the local domain relative to bulk. Thus, attractive electrostatic forces between the negatively charged DNA phosphates and sodium ions should decrease in aqueous urea and N-methylated glycine solutions and increase in ethylene glycol solutions, potentially determining the extent of sodium ion release.

Assuming the double-stranded DNA conformation is not changing with cosolute molality, then $\Delta n_{Na^+} = \Delta\xi^{-1} = \xi_c^{-1} - \xi_h^{-1}$, where ξ_c and ξ_h are the charge density parameters from Manning's counterion condensation model for the duplex (h) and single strands (c) (*44*, *46*). Since $\xi \sim 1/Db$, where D is the dielectric constant and b the axial charge spacing, $\Delta n_{Na^+} = \Delta\xi^{-1} \sim Db_c - Db_h$. Hence, a larger dielectric constant near the DNA surface should result in a larger Δn_{Na^+}. For ethylene glycol and a reduction in dielectric constant, Δn_{Na^+} should decrease with ethylene glycol molality. Since all of the cosolutes studied in this work are less excluded from the local domain of single-stranded DNA than double-stranded DNA, a larger perturbation of the local dielectric constant would be expected near the single-stranded DNA surface. Thus, the variation of Δn_{Na^+} between different cosolutes at a given water activity could depend not only on potential interaction of these cosolutes with DNA phosphates as in the case of the N-methylated glycines but also on the extent of local accumulation and dielectric constant dependence on cosolute molality (*45*).

DNA Hydration. The conformation of DNA is intimately tied to hydration. Formation of the double helix from single strands is accompanied by an uptake of about five waters per base pair in the hydration shell of DNA (*47*, *48*). Spink and Chaires (*1*) demonstrated that the major effect of cosolutes on DNA melting transitions is caused by changes in water activity, not bulk dielectric constant. These authors also used ethylene glycol, glycerol, acetamide, and sucrose as probes of DNA hydration changes during melting using thermodynamic linkage concepts. This thermodynamic analysis yielded approximately four waters released per base pair during the melting transition in ethylene glycol, glycerol, and acetamide aqueous solutions, in good agreement with calorimetric and neutron scattering studies (*47*, *48*). Statistically, the same number of waters was released in the melting transition for *E. coli* and poly(dA)·poly(dT) DNA (*1*). However, almost twice as many waters of hydration were released during the melting transition in aqueous sucrose solutions, an indication of a specific cosolute−DNA interaction.

The number of waters released in the melting transition can be expressed as

$$-\frac{\Delta H^\circ_{T_m}}{R}\left(\frac{d T_m^{-1}}{d \ln a_1}\right) = \Delta n_1 \qquad (10)$$

where a_1 is the activity of water and Δn_1 is the number of waters released per base pair in the DNA melting process (*1*). Comparison of eqs 4 and 10 indicates that changes in cosolute distribution in the local domain must be balanced by changes in water distribution. In the case of urea and ethylene glycol, constant values of $dT_m^{-1}/(d \ln a_1)$ (Figure 1) indicate constant differences in waters of hydration between single-stranded and double-stranded DNA.

Figure 8 shows a plot of Δn_1 versus GC content for the cosolutes ethylene glycol and urea. Values of Δn_1 for ethylene glycol are comparable to those measured by Spink and Chaires (*1*). Ethylene glycol $\Delta\Gamma_{\mu_3,m_4}/m_3$ and K_p values in Table 2 are mostly independent of GC content, indicating no differential specific interactions of this cosolute with either G, C, A, or T bases. Interestingly, Δn_1 has a minimum at 42% DNA GC content, with maximum values at 0% and 100% GC base pairs. This trend in Δn_1 agrees with the prediction of Chalikian and co-workers (*26*), using densimetric and ultrasonic techniques, that maximum hydration of the DNA double helix occurs at 0% and 100% GC content with minimum hydration at 50% GC content.

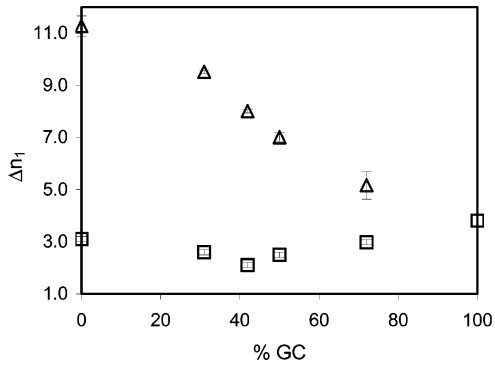

FIGURE 8: Number of waters released per base pair, Δn_1, as a function of GC content in aqueous ethylene glycol (□) and urea (△) solutions. Buffer conditions as in Figure 1.

In the case of urea, $\Delta\Gamma_{\mu_3,m_4}/m_3$ and K_p values (Table 2) decrease dramatically as GC content is increased. Urea has a strong preference for A and T bases, competing with water for binding sites along DNA, resulting in a larger dehydration than for G and C bases (Figure 8). Chalikian et al. (*26*) proposed that water is more tightly bound around GC base pairs in the double helix. If the affinity of water for G and C bases in single-stranded DNA is similar to that for GC base pairs, a larger dehydration of A and T bases should be expected with urea. The potentially weaker hydration of A and T bases may explain the higher accumulation of urea in the local domain surrounding single-stranded AT-rich DNA (Table 2), which in turn explains the greater instability of AT-rich double-stranded DNA in the presence of urea.

REFERENCES

1. Spink, C. H., and Chaires, J. B. (1999) Effects of hydration, ion release, and excluded volume on the melting of triplex and duplex DNA, *Biochemistry 38*, 496−508.
2. Del Vecchio, P., Esposito, D., Ricchi, L., and Barone, G. (1999) The effects of polyols on the thermal stability of calf thymus DNA, *Int. J. Biol. Marcomol. 24*, 361−369.
3. Blake, R. D., and Delcourt, S. G. (1996) Thermodynamic effects of formamide on DNA stability, *Nucleic Acids Res. 24*, 2095−2103.
4. Barone, G., Del Vecchio, P., Esposito, D., Fessas, D., and Graziano, G. (1996) Effect of osmoregulatory solutes on the thermal stability of calf-thymus DNA, *J. Chem. Soc., Faraday Trans. 92*, 1361−1367.
5. Rees, W. A., Yager, T. D., Korte, J., and von Hippel, P. H. (1993) Betaine can eliminate the base pair composition dependence of DNA melting, *Biochemistry 32*, 137−144.
6. Wang, C., Altieri, F., Ferraro, A., Giartosio, A., and Turano, C. (1993) The effect of polyols on the stability of duplex DNA, *Physiol. Chem. Phys. Med. NMR 25*, 273−280.
7. Klump, H., and Burkart, W. (1977) Calorimetric measurements of the transition enthalpy of DNA in aqueous urea solutions, *Biochim. Biophys. Acta 475*, 601−604.
8. Hong, J., Capp, M. W., Anderson, C. F., Saecker, R. M., Felitsky, D. J., Anderson, M. W., and Record, M. T., Jr. (2004) Preferential interactions of glycine betaine and of urea with DNA: implications for DNA hydration and for effects of these solutes on DNA stability, *Biochemistry 43*, 14744−14758.
9. Record, M. T., Jr., Zhang, W., and Anderson, C. F. (1998) Analysis of effects of salts and uncharged solutes on protein and nucleic acid equilibria and processes: a practical guide to recognizing and interpreting polyelectrolyte effects, Hofmeister effects, and osmotic effects of salts, *Adv. Protein Chem. 51*, 281−353.
10. Parsegian, V. A., Rand, R. P., and Rau, D. C. (2000) Osmotic stress, crowding, preferential hydration, and binding: a comparison of perspectives, *Proc. Natl. Acad. Sci. U.S.A. 97*, 3987−3992.
11. Shimizu, S. (2004) Estimating hydration changes upon biomolecular reactions from osmotic stress, high pressure, and preferential hydration measurements, *Proc. Natl. Acad. Sci. U.S.A. 101*, 1195−1199.
12. Babayan, Y. S. (1988) Conformation and thermostability of double-helical nucleic acids in aqueous solutions of urea, *Mol. Biol. 22*, 1204−1210.
13. Aslanyan, V. M., Babayan, Y. S., and Arutyunyan, S. G. (1984) Conformation and thermostability of DNA in aqueous urea solutions, *Biophysics 29*, 410−414.
14. Hong, J., Capp, M. W., Anderson, C. F., and Record, M. T. (2003) Preferential interactions in aqueous solutions of urea and KCl, *Biophys. Chem. 105*, 517−532.
15. Felitsky, D. J., and Record, M. T., Jr. (2004) Application of the local-bulk partitioning and competitive binding models to interpret preferential interactions of glycine betaine and urea with protein surface, *Biochemistry 43*, 9276−9288.
16. Tang, K. E. S., and Bloomfield, V. A. (2002) Assessing accumulated solvent near a macromolecular solute by preferential interaction coefficients, *Biophys. J. 82*, 2876−2891.
17. Courtenay, E. S., Capp, M. W., Saecker, R. M., and Record, M. T., Jr. (2000) Thermodynamic analysis of interactions between denaturants and protein surface exposed on unfolding: interpretation of urea and guanidinium chloride m-values and their correlation with changes in accessible surface area (ASA) using preferential interaction coefficients and the local-bulk domain model, *Proteins: Struct., Funct., Genet. 4*, 72−85.
18. Felitsky, D. J., Cannon, J. G., Capp, M. W., Hong, J., Van Wynsberghe, A. W., Anderson, C. F., and Record, M. T., Jr. (2004) The exclusion of glycine betaine from anionic biopolymer surface: why glycine betaine is an effective osmoprotectant but also a compatible solute, *Biochemistry 43*, 14732−14743.
19. Courtenay, E. S., Capp, M. W., Anderson, C. F., and Record, M. T. J. (2000) Vapor pressure osmometry studies of osmolyte-protein interactions: implications for the action of osmoprotectants in vivo and for the interpretation of "osmotic stress" experiments in vitro, *Biochemistry 39*, 4455−4471.
20. Felitsky, D. J., and Record, M. T., Jr. (2003) Thermal and urea-induced unfolding of the marginally stable lac repressor DNA-binding domain: a model system for analysis of solute effects on protein processes, *Biochemistry 42*, 2202−2217.
21. Wyman, J. (1965) The binding potential, a neglected linkage concept, *J. Mol. Biol. 11*, 631−644.
22. Wyman, J. J. (1964) Linked functions and reciprocal effects in hemoglobin: a second look, *Adv. Protein Chem. 19*, 223−286.
23. Moore, W. J. (1972) Solutions, in *Physical Chemistry*, Prentice-Hall, Upper Saddle River, NJ.
24. Schellman, J. A. (1990) A simple model for solvation in mixed solvents: applications to the stabilization and destabilization of macromolecular structures, *Biophys. Chem. 37*, 121−140.
25. Chaires, J. B., Ren, J., Henary, M., Zegrocka, O., Bishop, G. R., and Strekowski, L. (2003) Triplex selective 2-(2-naphthyl)-quinoline compounds: origins of affinity and new design principles, *J. Am. Chem. Soc. 125*, 7272−7283.
26. Chalikian, T. V., Sarvazyan, A. P., Plum, G. E., and Breslauer, K. J. (1994) Influence of base composition, base sequence, and duplex structure on DNA hydration: apparent molar volumes and apparent molar adiabatic compressibilities of synthetic and natural DNA duplexes at 25 °C, *Biochemistry 33*, 2394−2401.
27. Moore, W. J. (1972) Chemical Affinity, in *Physical Chemistry*, Prentice-Hall, Upper Saddle River, NJ.
28. Wolf, A. V., Brown, M. G., and Prentiss, P. G. (1978) Concentrative properties of aqueous solutions: conversion tables, in *CRC Handbook of Chemistry and Physics* (Weast, R. C., Ed.) pp D219−D276, CRC Press, Boca Raton, FL.
29. Scatchard, G., Hamer, W. J., and Wood, S. E. (1938) Isotonic solutions. I. The chemical potential of water in aqueous solutions of sodium chloride, potassium chloride, sulfuric acid, sucrose, urea and glycerol at 25°, *J. Am. Chem. Soc. 60*, 3061−3070.
30. Smith, E. R. B., and Smith, P. K. (1937) The activity of glycine in aqueous solution at twenty-five degrees, *J. Biol. Chem. 117*, 209−216.
31. Smith, P. K., and Smith, E. R. B. (1937) Thermodynamic properties of solutions of amino acids and related substances. II. The activity of aliphatic amino acids in aqueous solution at twenty-five degrees, *J. Biol. Chem. 121*, 607−613.
32. Smith, P. K., and Smith, E. R. B. (1940) Thermodynamic properties of solutions of amino acids and related substances. V.

The activities of some hydroxy- and *N*-methylamino acids and proline in aqueous solution at twenty-five degrees, *J. Biol. Chem. 132*, 57−64.
33. Chalikian, T. V., Volker, J., Plum, G. E., and Breslauer, K. J. (1999) A more unified picture for the thermodynamics of nucleic acid duplex melting: a characterization by calorimetric and volumetric techniques, *Proc. Natl. Acad. Sci. U.S.A. 96*, 7853−7858.
34. Karapetian, A. T., Vardevanian, P. O., and Frank-Kamenetskii, M. D. (1990) Enthalpy of helix-coil transition of DNA: dependence on Na^+ concentration and GC-content, *J. Biomol. Struct. Dyn. 8*, 131−138.
35. Gruenwedel, D. W. (1974) Salt effects on the denaturation of DNA. III. A calorimetric investigation of the transition enthalpy of calf thymus DNA in Na_2SO_4 solutions of varying ionic strength, *Biochim. Biophys. Acta 340*, 16−30.
36. Hultgren, A., and Rau, D. C. (2004) Exclusion of alcohols from spermidine-DNA assemblies: probing the physical basis of preferential hydration, *Biochemistry 43*, 8272−8280.
37. Flock, S., and Houssier, C. (1997) Effect of glycine on DNA structural transitions induced by multivalent cationic compounds, *J. Biomol. Struct. Dyn. 15*, 53−61.
38. Flock, S., Labarbe, R., and Houssier, C. (1995) Osmotic effectors and DNA structure: effect of glycine on precipitation of DNA by multivalent cations, *J. Biomol. Struct. Dyn. 13*, 87−102.
39. Aslanyan, V. M., and Arutyunyan, S. G. (1985) Conformational state of DNA in aqueous solutions containing glycine, β-alanine, and γ-aminobutyric acid. Temperature effect, *Biofizika 30*, 741−745.
40. Aslanyan, V. M., and Arutyunyan, S. G. (1985) Conformational state of DNA realized in aqueous solutions of glycine, β-alanine, and γ-aminobutyric acid. DNA conformational transitions stimulated by alkali metal ions, *Biofizika 30*, 746−749.
41. Rajendrakumar, C. S. V., Suryanarayana, T., and Reddy, A. R. (1997) DNA helix destabilization by proline and betaine: possible role in the salinity tolerance process, *FEBS Lett. 410*, 201−205.
42. Timasheff, S. N. (1993) The control of protein stability and association by weak interactions with water: how do solvents affect these processes?, *Annu. Rev. Biophys. Biomol. Struct. 22*, 67−97.
43. Santoro, M. M., Liu, Y., Khan, S. M. A., Hou, L.-X., and Bolen, D. W. (1992) Increased thermal stability of proteins in the presence of naturally occurring osmolytes, *Biochemistry 31*, 5278−5283.
44. Record, M. T. J., Anderson, C. F., and Lohman, T. M. (1978) Thermodynamic analysis of ion effects on the binding and conformational equilibria of proteins and nucleic acids: the roles of ion association or release, screening, and ion effects on water activity, *Q. Rev. Biophys. 11*, 103−178.
45. Edsall, J. T. (1943) Dielectric constants and dipole moments of dipolar ions, in *Proteins, Amino Acids, and Peptides as Dipolar Ions* (Cohn, E. J., and Edsall, J. T., Eds.) pp 140−154, Reinhold Publishing Co., New York.
46. Manning, G. S. (1978) The molecular theory of polyelectrolyte solutions with applications to the electrostatic properties of polynucleotides, *Q. Rev. Biophys. 11*, 179−246.
47. Bastos, M., Castro, V., Mrevlishvili, G., and Teixeira, J. (2004) Hydration of ds-DNA and ss-DNA by neutron quasielastic scattering, *Biophys. J. 86*, 3822−3827.
48. Mrevlishvili, G. M., Carvalho, A. P. S. M. C., and da Silva, M. A. V. R. (2002) Low-temperature DSC study of the hydration of ss-DNA and ds-DNA and the role of hydrogen-bonded network to the duplex transition thermodynamics, *Thermochim. Acta 394*, 73−82.

BI052469I